Quantifying trailing edge flap control capability on wind turbines in a controlled environment

Farid Samara * and David A. Johnson†
University of Waterloo, 200 University Ave W, Waterloo, Canada N2L 3G1

As wind turbine diameters continue to increase, the cyclic loading experienced by the turbine blade due to wind shear and yaw misalignment increases dramatically hindering the development of larger more efficient turbines. Based on current literature, controlling a section of the trailing edge of the turbine blade was found to reduce cyclic loading. To quantify the load control capability of a trailing edge flap (TEF), an experimental rig was designed to evaluate a TEF on a 3.5 m diameter wind turbine operating under different tip speed ratios, yaw angles and blade pitch angles inside a large wind generation facility. The TEF was tested at two different spanwise locations r/R=0.66 and 0.82. The instrumented blade was capable of measuring rotor torque, flapwise/edgewise blade root bending moment, and normal force coefficient at two different spanwise locations r/R=0.66 and 0.82. The experimental results show that the use of a TEF was capable of manipulating the normal force coefficient by 40% and the flapwise bending moment by 20%. The relationship between the TEF angle and both blade bending moment and normal force coefficient was linear for all the cases tested. The results also show that when the TEF was centered at r/R=0.82 it could control the turbine loading more effectively. The results presented here prove that the TEF is capable of reducing cyclic loading on wind turbine blades.

Nomenclature

α	=	angle of attack, deg
α_F	=	trailing edge flap angle, deg
β	=	blade pitch angle, deg
γ	=	yaw angle, deg
λ	=	tip speed ratio
ψ	=	azimuth position, deg
ζ	=	a constant function of airfoil geometry

*Ph.D., Wind Energy Group, Mechanical and Mechatronics Engineering; fsamara@uwaterloo.ca
†Professor, Wind Energy Group, Mechanical and Mechatronics Engineering; david.johnson@uwaterloo.ca

Samara, F., & Johnson, D. A. (2021). Quantifying Trailing Edge Flap Control Capability on Wind Turbines in a Controlled Environment. AIAA Journal, 1–11.
https://doi.org/10.2514/1.J060106

C_L = coefficient of lift

C_n = normal force coefficient

C_p = coefficient of pressure

M_{FW} = blade root flapwise moment, Nm

M_{EW} = blade root edgewise moment, Nm

c = airfoil chord, m

r = radius of a point on the blade , m

R = blade tip radius, m

STD = standard deviation

TEF = trailing edge flap

TE = trailing edge

LE = leading edge

I. Introduction

Wind energy, an established renewable source of energy, has realized significant growth over the last several decades mainly due to substantial innovation in turbine design that has been able to increase energy production while simultaneously reduce wind farm costs [1]. Recent trends show that the size and diameter of wind turbines have been steadily increasing over the years, partly driven to decrease cost and capture more energy [2, 3]. One of the main problems that arises as the wind turbine rotor diameter increases is due to the environmental operating conditions. It is understood that wind turbines spend most of the time in a relatively unsteady flow environment caused by many factors including wind shear and yaw misalignment to name a couple [4, 5]. Wind turbines experience yaw misalignment between the rotor axis and the wind direction on a regular basis because the rotor is not always capable of following the continuously changing wind direction. Therefore turbines spend most of their time in yawed conditions. Also, in recent years, wind farm operators have been considering intentionally yawing turbines to redirect the wake away from downstream turbines to increase the efficiency of the entire wind farm [1, 6, 7]. A yawed turbine causes a significant increase in fatigue loads at the blade root and that hinders operators from actively pursuing wake redirection. Yaw misalignment also causes flow unsteadiness and that in turn leads to load fluctuation on the blades causing material fatigue while decreasing the lifespan of the blades. In general, even though static loads could be higher than these load fluctuations, the latter tends to be more problematic due to material fatigue and fatigue life governs the design factors for larger wind turbines [3]. As the blades get longer, the load fluctuation at the root increases substantially causing higher material fatigue levels. Thus more research should be aimed at finding new techniques to reduce load fluctuation and cyclic loading.

Many research groups have been focusing on developing active aerodynamic modification techniques to reduce load fluctuation and material fatigue. Active modification of the blade shape, also known as 'Smart Rotor', could lead to cost reduction of the blades, towers and drive train [3]. This would enable the industry to build larger wind turbines using less material in the blade design, making them lighter and increasing the operational-life expectancy of the rotor thus reducing levelized cost of energy [8]. Active blade modification would be based on information obtained from different sensors embedded in the wind turbine that measure blade loading. The recent "Grand Vision for Wind Energy" by Dykes *et al.* [1] identified key challenges that must be addressed to realize the future potential of wind power. One of the many opportunities discussed was advances in active aerodynamic control and remote sensing that could reduce cyclic loading on the turbine. This will enable future blades to be even longer, lighter and most importantly reducing the fatigue levels of the blades while still adhering to the safety standards required. In summary, developing wind turbine load reduction techniques could increase the power produced by the turbine, reduce the capital and maintenance cost while prolonging the lifespan of the system.

Different blade cyclic load reduction strategies have been developed previously such as leading edge blowing or suction, synthetic jets, leading edge plasma actuation, vortex generators and trailing edge flaps (TEF). Barlas and van Kuik [3] summarized and reviewed the different control strategies mentioned to reduce blade fatigue loading. TEF was found to be the most efficient of the control strategies tested because of its control capability over the coefficients of lift and drag, linearity, high frequency response and their simplicity of use. In comparison, they found: microtabs are less efficient for detailed load control due to their on-off characteristics; camber control is expensive, complex to design, and has high power consumption; and boundary layer strategies are limited by their control capability. Samara and Johnson [9, 10] investigated the use of a TEF to reduce the load fluctuation on a pitching 2D airfoil in a wind tunnel. They found that the TEF was capable of reducing the cyclic fluctuation in the coefficient of lift and root bending moment by at least 26% and 24%, respectively. Moreover, a similar experimental blade setup will be utilized in this experiment on a full scale wind turbine. Samara and Johnson [11] briefly studies how the TEF influences average wind turbine loading. In this article, time resolved turbine loading is presented versus azimuth position.

Abdelrahman and Johnson [12] investigated the influence of TEF on a 3.4 m diameter wind turbine in a controlled environment. The TEF occupied 20% of the chord and 15% of the 1.7 m long blade. The TEF was placed at different locations along the blade radius and the results showed that the TEF influence over blade load control is largest when it is located at *r/R*=0.89 (where r is the radius of a point on the blade and R is the blade tip radius). When deflecting the TEF angle (α_F) to +15° and -15° at *r/R*=0.89, the blade root flapwise moment (M_{FW}) changed by -15% and +20% respectively. It was concluded that the relationship between α_F and M_{FW} was relatively linear except the fact that $-\alpha_F$ had a larger control capability than $+\alpha_F$. Even though the experimental campaign was successful, a few key parameters were missing: the TEF was not automated and it was deflected manually, the data acquisition system was not capable of phase averaging the data to study load fluctuation with azimuth and more importantly surface pressure measurements

were not measured.

Berg *et al.* [13–17] designed, fabricated and tested a TEF on a utility-scale wind turbine with a blade length of 9 m. The TEF, designed to have a deflection of ±20°, occupied 20% of the chord and 20% of the blade span between *r/R*=0.78 and *r/R*=0.98. The results showed that the TEF was capable of decreasing the blade cyclic load fluctuation by 20%. The power from the wind turbine for different flap angles was compared to the unmodified wind turbine blades and the results show power output changed with flap angles for all wind speeds. This utility-scale test lacked surface pressure measurements along the blade and active control of the TEF to reduce load fluctuation. The study was mainly aimed at the design and mechanical components of the TEF and less on the aerodynamic aspects.

Miller and Quandt [18] designed and conducted a series of experiments on a full scale instrumented wind turbine to test the capability of a TEF in attenuating structural loads and increasing wind turbine efficiency in unsteady conditions. Based on the results they found, the normal force coefficient could be reduced by as much as 0.6 when the TEF is deflected to an extreme value of +90°. They then suggested that the TEF could be used to assist the pitch control of utility-scale turbines. That would reduce the stress and maintenance cost on the pitch system and that could offset the cost of TEF.

Andersen *et al.* [19] numerically simulated a wind turbine with a TEF to find the optimal location to place the flap where it could reduce load fluctuation the most. They concluded that depending on whether the blades are stiff (rigid in structure) or elastic (allowing the blade to slightly deform under load) the TEF should be located at *r/R*=0.94 and *r/R*=0.71, respectively. Usually beyond 90% the tip losses would dominate and the TEF is ineffective in that region. This would indicate that the ideal location for the TEF is dependent on the elasticity of the blade and in the current study, the blade is elastic because the blade did deform under load according to Samara [20]. Thus, according to Andersen *et al.*, placing the TEF around *r/R*=0.71 is ideal and in this study the TEF was placed at two r/R locations: 0.66 and 0.82.

Based on the literature review, there is a need to validate and calibrate the control capability of a TEF on a wind turbine blade in a controlled environment. Controlled experimental wind tunnel testing of scaled models has been used in the past to provide valuable turbine performance information to the research community. Two key scaled studies of the aerodynamics of wind turbines are the "Unsteady Aerodynamics Experiment Phase VI" project [21] and the "Mexnext MEXICO" project [22] on a similar scale to the research presented here. The latter two studies did not cover TEF but showed that wind tunnel testing could provide valuable insight into the aerodynamics of wind turbines. Wind tunnel testing did not exactly replicate full scale and field testing, but both worked in synergy towards the goal of delivering validated and calibrated data. In wind tunnel testing, it may be possible to perform measurements and obtain databases which might not be feasible at full scale. It is usually impossible to exactly match all the relevant physics between the scaled model and full scale due to limitations in scaling conditions. That being said, Canet *et al.* [23] argued relevant key aspects of the steady and unsteady response of the rotor can be indeed matched when up-scaling. They provided an in-depth analysis about how scaling influences the physics of the scaled model. In most instances the

Reynolds number cannot be matched when scaling down a wind turbine and according to them that is not a problem. When scaling down, the airfoils used to build the blades are different and are optimized to the scaled-down low Reynolds number. Canet *et al.* [23] showed that using this strategy, scaled rotors can confidently draw insight into large model full scale rotors. Bottasso *et al.* [24] both showed that testing scaled down wind turbines in wind tunnels do in fact provide insight about the aerodynamics on full scale wind turbines.

Experimental data on a full scale instrumented turbine with a TEF are scarce particularly in a controlled environment (wind tunnel testing). The experimental data provided here provides important information to improve aerodynamic understanding of a wind turbine equipped with a TEF. Having a complete and comprehensive set of experiments helps to shed some light on how a TEF manipulates rotor power, total blade loading and forces on a small blade segment. Furthermore, the experimental data will be an excellent resource for modelers to develop new models to simulate TEF on a wind turbine or to validate existing models.

A. Objective and Contributions

Based on the introduction, one could then understand the benefits of active aerodynamic control including reducing load fluctuation and fatigue levels on the blades. To do so, a solid understanding of how a TEF influences rotor loading when the turbine is operating under different conditions must be achieved and that is the main aim of this study. The objective is then to study how deflecting the TEF to fixed angles influences rotor torque, blade root flapwise bending moment (M_{FW}), normal force coefficient (C_n) and chordwise coefficient of pressure (C_p) at r/R=0.66 and 0.82. These variables are measured and presented for different turbine tip speed ratios (λ), blade pitch angles (β) and different rotor yaw angles (γ). The contribution of this study is in its experimental setup, multiple load measurement techniques and comprehensive test matrix in a controlled wind generation facility. Surface pressure measurements on a rotating blade equipped with a TEF have never been presented before thus providing new insight on how the TEF influences the aerodynamics around the blade. The fixed TEF angle database presented here could then be used to design a control strategy to reduce load fluctuation on a wind turbine and achieve active aerodynamic control.

II. Background and Theory

The most basic TEF is achieved by hinging the trailing edge (TE) about a point typically located between 0.7 to 0.9 of the chord. When the flap is deflected towards the pressure side (negative angle as illustrated in Figure 1) the coefficient of lift (C_L) increases due to the increase in camber of the airfoil. The opposite is true when the flap is deflected towards the suction side [25].

Thin airfoil theory has been used to predict the influence of TEF on the lift coefficient (C_L) and is described in more detail by Houghton and Carpenter [26]. Changing the flap angle is similar to modifying the camber of an airfoil and thus thin airfoil theory could be used to develop an equation for flapped airfoils. More detail about the development of

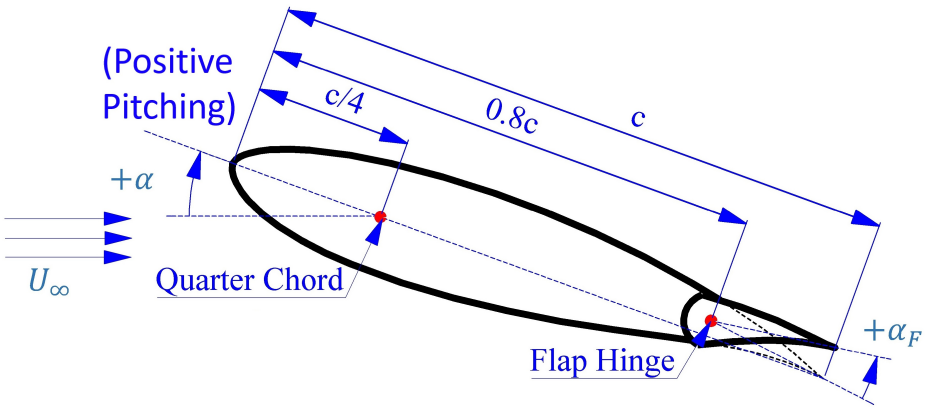

Fig. 1 A sketch illustrating the airfoil and angle of attack (α) and TEF flap angle (α_F) sign convention along with the positive pitching moment and free stream velocity (U_∞)

the equations and an in-depth analysis could be found in Houghton and Carpenter [26]. The modified equation derived to predict C_L for different flap angles is:

$$C_L = 2\pi\alpha + 2(\pi - \zeta + sin\zeta)\alpha_F \tag{1}$$

where ζ is a constant that is a function of airfoil geometry and α is the angle of attack. The first part, $2\pi\alpha$, accounts for the effect of the geometric angle of attack while the second part accounts for the camber and flap angle (α_F) of the airfoil. The change in C_L due to the flap could then be obtained from Equation (1) but with a limited accuracy. As with any equation derived from thin airfoil theory, the viscosity effects that are particularly prominent close to the TE are not accounted for by Equation (1). The theory also is limited to small α and small α_F thus experimental data are needed to obtain data at larger angles. The main conclusion to be drawn here is that the relationship between C_L and α_F is linear as long as the flow over the airfoil is attached.

Miller and Quandt [18] found that the TEF was more effective at controlling the aerodynamic loads in wind tunnel testing (2D infinite span) than in 3D testing where the blade is rotating. They attributed the difference between the 2D airfoil and the 3D blade to the fact that a new shed vortex is formed at the TE between the unmodified blade and the TEF section as shown in Figure 2. They suggested that this vortex was capable of significantly reducing α leading to a reduction in blade loading and performance. They also suggested that the load reduction could wrongly be attributed to the TEF aerodynamics when, in fact, it is occurring on the inboard section of the blade. They did not provide a quantitative effect of this newly formed vortex. Abdelrahman and Johnson [12] also suggested that the new vortex formed at the TEF/blade interface is similar to the tip vortex created at the tip of the blade that induces a decrease in α on the inboard (towards hub) segments of the blade.

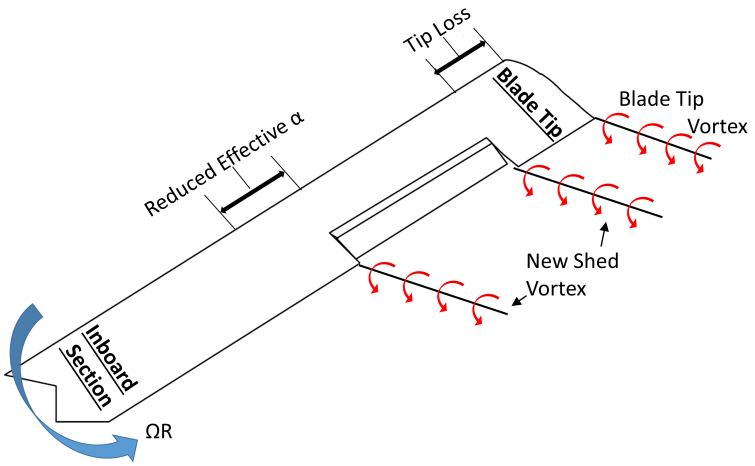

Fig. 2 The location of the newly developed vortex at the TEF where it reduces the effective α at the inboard section of the blade. Adapted from [18].

.

III. Methodology and Verification

A. Experimental Setup

The experimental campaign was conducted at the Wind Generation Facility operated by the University of Waterloo. It is a large scale open circuit wind tunnel with a test area of 15.4 m wide and 7.8 m high. The maximum achievable wind speed is 13 m/s but more importantly the blockage ratio is around 7% and the turbulence intensity is around 8%. The fully instrumented upwind horizontal-axis wind turbine with a 3.5 m diameter, shown in Figure 3, was used to measure the loads at three different locations on the turbine. First, the torque sensor in the drivetrain in the nacelle was used to measure the torque generated by the entire rotor. Second, strain gauges at the root of the blade were used to measure the flapwise (M_{FW}) and edgewise (M_{EW}) root bending moment. Finally, 27 differential pressure transducers located inside the blade profile were used to measure the the differential pressure between the suction and pressure side of the airfoil at the same chordwise location simultaneously. More details about this technique and how it was successfully validated could be found in Samara and Johnson [9]. The surface pressure taps were located at the center of the TEF as seen in Figure 3 and four of the taps were located on the flap itself. By integrating the surface pressure measurements, the normal force coefficient (C_n) was obtained. The 3.5 m diameter rotor consists of one aerodynamic blade and two thin counterweight cylinders (19 mm in diameter). Abdelrahman and Johnson [12] used a similar setup and found that even though the induction is reduced due to the use of one aerodynamic blade, the insight drawn from the single bladed turbine could be extended to the three bladed turbine. The aerodynamic blade is composed of an S833 airfoil with a constant chord of 178 mm and a constant pitch of $\beta = 6°$. The single-bladed turbine has only one TEF section that occupies 22% of the 1.47m aerodynamic blade or 19% of the 1.77m rotor radius. Since the blade design is modular, the TEF center section could be placed at two *r/R* locations, 0.82 and 0.66. The TEF blade section was

manually moved from one location to the other. When the TEF is centered at *r/R*=0.82, the flap is located between *r/R*=0.73 and 0.91. On the other hand, when the TEF centered at *r/R*=0.66, the flap is located between *r/R*=0.56 and 0.75. All the mentioned measurements were collected simultaneously and in time-resolved fashion so the data could be phase averaged and presented versus azimuth position (ψ). This was achieved through the custom integrated data acquisition (DAQ) system placed in the rotating hub and it was capable of sending the measured data from the sensors wirelessly to the stationary computer. A custom built pitch control and trailing edge flap (TEF) control were used to automate the position of the blade pitch and TEF angle remotely from the control room. Both systems were also designed to actuate the pitch and TEF in real time to mitigate turbine loads in unsteady conditions and these results will be presented in the future. Details about the experimental setup have been intentionally reduced here because the setup has been discussed in more detail by Samara and Johnson elsewhere [11, 20, 27].

To assess the error associated with the experimental results presented, uncertainty analysis was conducted. The maximum uncertainty in the flapwise (M_{FW}) or edgewise (M_{EW}) root bending moment was calculated to be ±0.5% of the measured value. The rotor torque measurements had a maximum uncertainty of ±0.3% full scale or ±0.6 N.m. The average representative uncertainty in C_n was calculated to be ±0.069 and error bars are used in the results to show the uncertainty at each data point. Uncertainty in ΔC_p was calculated to be ±0.085. The uncertainty was based on the error in the pressure transducers and wind tunnel velocity. The uncertainty in α and TEF angle is ±0.1° and ±2°, respectively. Further details regarding the uncertainty analysis could be found in Samara [20].

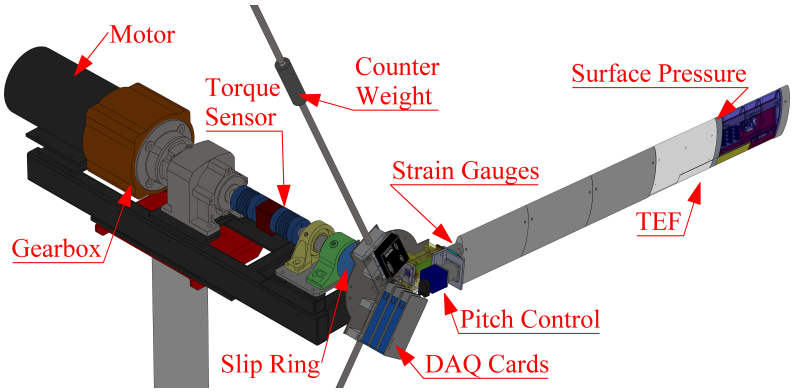

Fig. 3 3D model of the wind turbine assembly showing the main components

B. Test Matrix

A comprehensive test matrix was developed to understand how the TEF influences blade aerodynamics. Two yaw angles, $\gamma = 0°$ and 30°, were chosen to simulate steady and unsteady wind turbine aerodynamics. The unsteady case was used to determine how the control capability of the TEF changes when the blade is operating in stall. Two blade pitch angles (β= 3° and 6°) and three different tip speed ratios (λ = 3.5, 4.2 and 5) were tested to study TEF aerodynamics while the turbine is operating under different conditions. These λ values were also chosen to match the experiments

conducted by Gallant and Johnson [28] and Abdelrahman and Johnson [12]. The flap angle, α_F, ranged from -20° to 20° in steps of 10° to study the load control capability of the TEF. The TEF was also evaluated at two different spanwise locations (r/R=0.82 and 0.66) to study how the change in TEF location influences blade loading, provide a second data set and to determine which of the two locations is more efficient for the TEF to alleviate cyclic loading on the blade. The combination of all the variables tested is equivalent to 120 individual experiments. This large number measurement campaign matrix provides more detailed insight into wind turbine aerodynamics under a wide range of operating conditions.

The complete set of experiments are not all reported here. Out of the 120 tests conducted, only the most interesting and informative cases are plotted. To better understand and more effectively highlight the TEF impact, a matrix was created grouping the different tests into 5 cases and they are listed in Table 1. For *Case b.R2*, the TEF was deflected to large angles of ±80° to study how a TEF could force the blade section to stall and how that influences blade loading. The influence of TEF on a non-yawed wind turbine under different wind speeds and blade pitch angles is presented first followed by the same set of conditions but on a yawed turbine. The three variables that are studied and plotted against azimuth are: rotor torque, flapwise root bending moment (M_{FW}), normal force coefficient (C_n) and surface pressure coefficient (ΔC_p). The figure reference link in the table is added for organizational purposes.

Table 1 Test matrix for steady flap angle for different wind turbine operating conditions

Case	λ	$\beta(^\circ)$	TEF *r/R* Location	$\alpha_F(^\circ)$	$\gamma(^\circ)$	Variables Presented	Figure Reference
a	5	6	0.82	[-20:10:20]	0	ΔTorque, M_{FW}, C_n	Figure 4
b.R1	3.5	3	0.82	[-20:10:20]	0	ΔTorque, M_{FW}, C_n , ΔC_p	Figure 5 and 7
b.R2	3.5	3	0.66	[-80:20:80]	0	average{ΔTorque, M_{FW}, C_n} , ΔC_p	Figure 8 and 9
c	3.5	3	0.82	[-20:10:20]	30	ΔTorque, M_{FW}, C_n, ΔC_p	Figure 10 and 11

For all the plots presented in this study, rotor ΔTorque is plotted instead of rotor torque to highlight the torque generated by the single-blade and eliminate the measured drag generated by the counterweight cylinders. Rotor ΔTorque is the difference between the measured torque with no wind and the measured torque when the wind speed is set to the desired speed. The measured torque with no incoming wind is 29 Nm when the turbine rotation is set to 200 rpm. This means that if ΔTorque is greater than 29 Nm then the rotor torque is positive but if it is less than 29 Nm then the rotor torque is negative and the motor in the nacelle is driving the rotor. Since ΔTorque in all the cases presented is less than 29 Nm, this indicates that the single-bladed rotor is not capable of providing sufficient rotational force to overcome drag and other losses (like the gearbox and bearing) at the specified rotational speed.

IV. Results

This study focuses on developing an understanding of how the TEF influences wind turbine loading under different blade pitch angles, yaw angles, tip speed ratios and *r/R* locations to simulate different operating conditions. The results here are compared to other experimental work when data is available. First, for *Case a*, a set of plots are presented to show how the wind turbine performance parameters change with fixed flap angles for a non-yawed turbine representative of steady conditions. The TEF was then tested at two different spanwise locations *r/R*=0.82 and 0.66 (*Case b.R1* and *b.R2*) to find which of these two locations is better at controlling wind turbine loading. Finally for *Case c*, the same set of plots are presented for a yawed turbine to study how the TEF control capability changes in yawed conditions.

A. Yaw=0° Flap at *r/R*=0.82

Case a is presented first where the turbine performance parameters are plotted against azimuth (ψ) in Figure 4 where $\beta = 6°$, $\gamma = 0°$, λ=5 and the flap is centered at *r/R*=0.82. All the variables presented are phase-averaged from 1000 cycles into bins of 5° and all data is plotted with only every 4$^{\text{th}}$ data point marked with a symbol for clarity. Error bars were added for the M_{FW} and C_n plots only because the error in ΔTorque was found to be negligible due to the low instrumentation error and high number of data points collected. The error bars in the M_{FW} plots are very small indicating that the error could be ignored. The error bars in the C_n plots are significant because of the precision error (small) and unsteady flow events. A dynamically stalled blade causes a significant variation in measured parameters that could manifest itself in the error bars plotted. Focusing on the ΔTorque measurements in Figure 4a, $\alpha_F = -20°$ slightly increased rotor power by 4.4% while $\alpha_F = 20°$ substantially decreased rotor power by 19.5%. Apart from the change in lift coefficient as the flap angle changes, the drag coefficient (C_D) plays an important role in determining rotor torque. Abbott and Von Doenhoff [29] in a 2D flow study showed that $+\alpha_F$ increased C_D significantly but $-\alpha_F$ has only a slight impact on C_D. This explains why $+\alpha_F$ caused a significant reduction in ΔTorque because of the higher drag coefficient created by the TEF blade segment. Berg *et al.* [17] reported similar findings on a utility-scale turbine for the same flap angle deflections and for the same λ. They found that for high λ values, $-\alpha_F$ slightly increased turbine power output while $+\alpha_F$ significantly reduced power output. This shows that positive power augmentation from $-\alpha_F$ angles is very useful in low wind speed conditions because it increases the power production of the wind turbine.

The blade flapwise moment, M_{FW}, is presented next in Figure 4b where $+\alpha_F$ reduces blade loading while $-\alpha_F$ does the opposite. The increase in M_{FW} for all the presented cases at $\psi \approx 85°$ and $\approx 270°$ is due to the small spatial variation in wind speed in the large wind facility. This non-uniformity has been characterized and observed by Gallant [30] and McKinnon [31] and is present in all subsequent $M_{FW} - \psi$ plots. The change in M_{FW} for $\alpha_F = -20°$ and 20° relative to 0° is +19% and -22%, respectively. The control capability of $-\alpha_F$ is then found to be slightly lower than the control capability of $+\alpha_F$ due to the upper limit in the lift coefficient and the tendency for the airfoil to stall for high $-\alpha_F$ values. Berg *et al.* [17], measuring only M_{FW} and not C_n, found a similar trend in their data. This effect is

also seen in the C_n plots in Figure 4c, where the change in C_n for $\alpha_F = -20°$ and $20°$ relative to $0°$ is 36% and -39%, respectively. A more detailed discussion about the difference between $+\alpha_F$ and $-\alpha_F$ follows the presentation of Figure 6. There is a larger change in C_n than in M_{FW} because the latter measures loading on the entire blade where the TEF only occupies 22% of the blade span, while C_n measures the local forces at the midspan of the TEF segment. The slight variation in $C_n - \psi$ is due to the small spatial variation in wind speed in the large wind facility that was also seen in the $M_{FW} - \psi$ plot. In all cases, this slight non-uniformity appears in the same location.

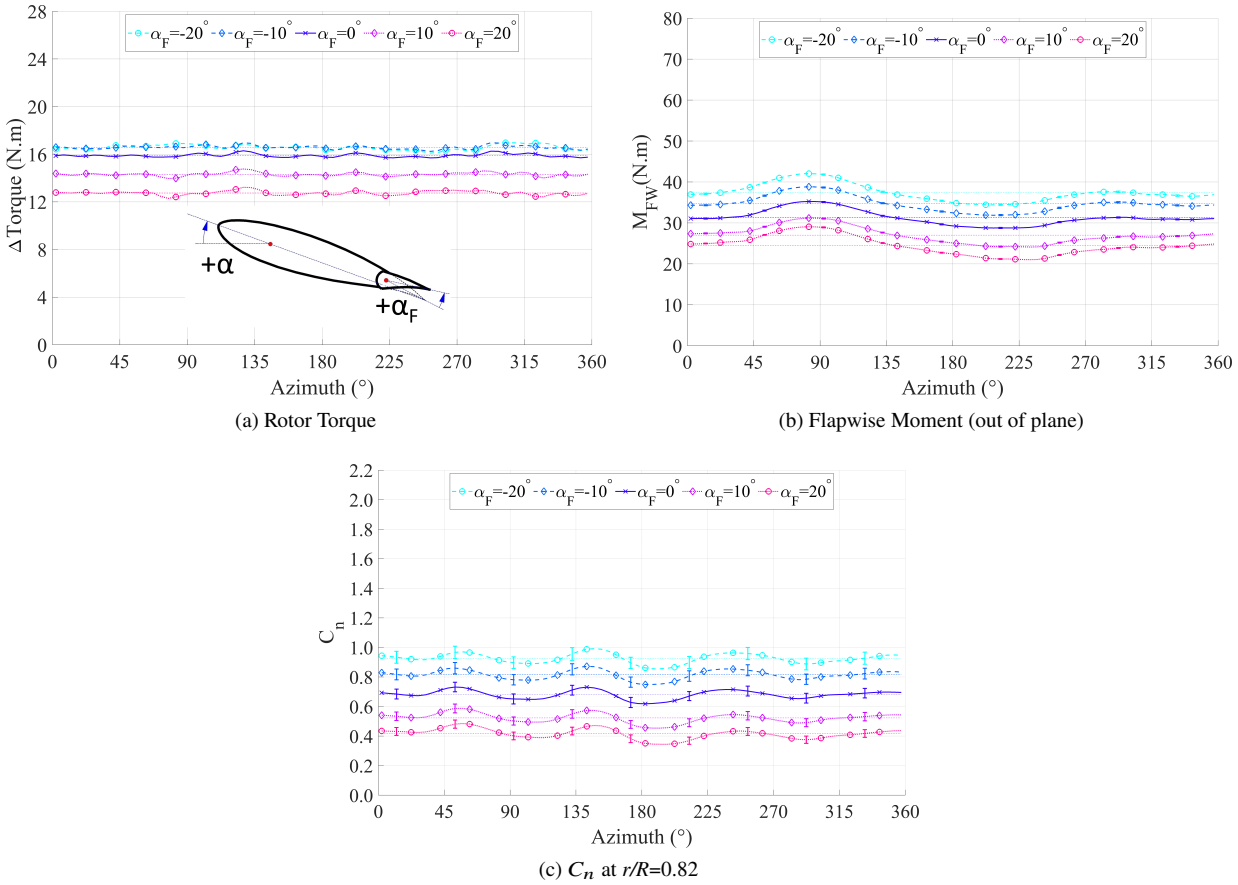

(a) Rotor Torque

(b) Flapwise Moment (out of plane)

(c) C_n at *r/R*=0.82

Fig. 4 Turbine performance for various α_F for *Case a* where $\beta = 6°$, $\gamma = 0°$, $\lambda = 5$ and the flap is centered at *r/R*=0.82. All data is plotted with only every 4th data point marked with a symbol for clarity.

To study how the blade pitch and wind speed change the flap control capability, *Case b.R1* is presented in Figure 5 where β decreased from 6° to 3° and λ decreased from 5 to 3.5. Figure 5a shows that there was no increase in ΔTorque at all for $-\alpha_F$ but for positive angles the same reduction shift is still present when compared to *Case a*. This result could be due to the larger forces experienced by the rotor when the wind speed increased. Decreasing the blade pitch from 6° to 3° also forces a larger section of the blade to stall, significantly increasing the drag coefficient. The results from Berg *et al.* [17] also show that at lower wind speeds, $-\alpha_F$ slightly increases rotor power but for higher wind speeds there is no change in rotor power. As mentioned above, the data collected here, from a scaled down wind turbine tested inside a

wind tunnel, showed a very similar behavior to the data collected from the Berg *et al.* [17] full scale wind turbine tested in the field. This would indicate that the physics obtained from a properly scaled-down wind turbine can indeed be used to obtain insight about full scale turbines as in this case. Although wind tunnel testing cannot exactly reproduce full scale results nor replace field measurements, it does play an important role in validating the control capability of the TEF on a full scale wind turbine.

From the M_{FW} and C_n data (Figures 5b and 5c), similar conclusions can be drawn. The absolute shift in value of these two variables for different α_F angles did not change (within uncertainty limits) from *Case a* to *b.R1* but the percentage change did differ. A more detailed comparison between *Case a* and *b.R1* is presented next in Figure 6. Another important observation to note is that the TEF shifted the turbine loading for the entire cycle and all azimuth positions equally. This observation demonstrates that the methodology used to collect turbine performance parameters is reliable and repeatable even though some of the data were collected on different days.

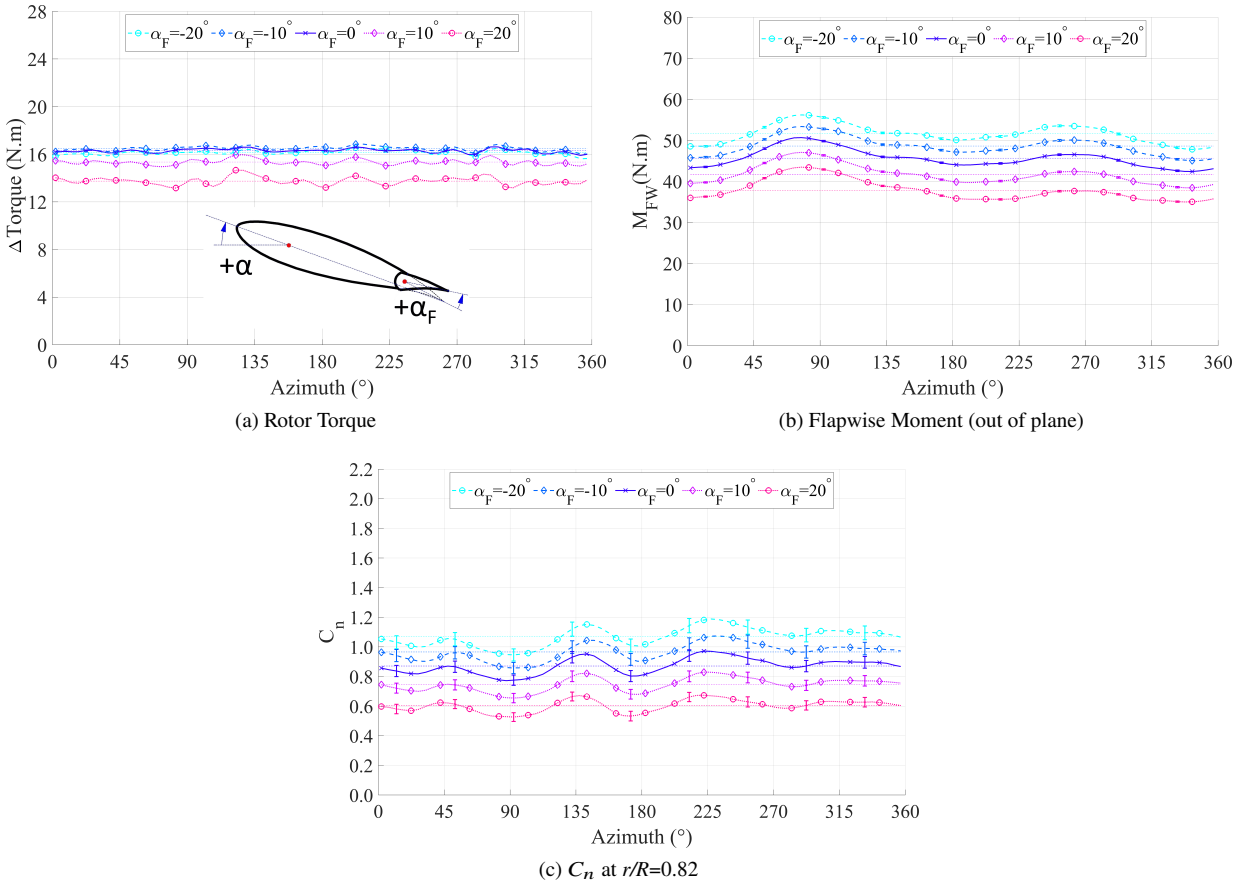

(a) Rotor Torque

(b) Flapwise Moment (out of plane)

(c) C_n at *r/R*=0.82

Fig. 5 Turbine performance for various α_F for *Case b.R1* where $\beta = 3°$, $\gamma = 0°$, λ=3.5 and the flap is centered at *r/R*=0.82. All data is plotted with only every 4th data point marked with a symbol for clarity.

To better understand how α_F influences the aerodynamics of the blade and how it compares to a 2D airfoil section, Figure 6 plots the percentage change in M_{FW} and C_n relative to $\alpha_F = 0°$. The 2D static wind tunnel experimental data

for the S833 airfoil with the same TEF dimensions has been obtained from Samara and Johnson [9]. Both plots clearly show that the C_n and M_{FW} percent change versus α_F slope decreases as the wind speed increases or β decreases (going from *Case a* to *Case b.R1*). This change in slope occurs because the aerodynamic loading on the turbine increases with the latter two variables. The TEF could manipulate loading by a certain amount and that change in load is not influenced by a change in λ or β. So when turbine loading increases due to the latter two variables, the influence of the TEF decreases because the change in load due to the TEF becomes less significant. The control capability for $-\alpha_F$ is less than that for $+\alpha_F$ due to the upper limit in the lift coefficient and the tendency for the airfoil to stall for high $-\alpha_F$ as discussed earlier and is seen on the turbine blade and 2D static cases. Abdelrahman and Johnson [12] conducted a similar experiment on the same single-bladed turbine using the same airfoil and dimensions but they only reported cycle-averaged values for M_{FW}. One of the main differences between their experiment and this experiment is the added value of phase-averaging (plotting the data versus ψ) of the current data and collecting surface pressure measurements to obtain C_n. Their results are also plotted in Figure 6 for comparison. The trends in their data align very well with the data collected in this experiment. This increases confidence in the data and conclusions made. Some of the differences between the two experiments could be due to the location and length of the flap or experimental uncertainties. The flap length they used was 0.25 m centered around *r/R*=0.89 whereas the flap length reported here was 0.33 m, centered around *r/R*=0.82.

Another important note to emphasize is that the relationship between $M_{FW} - \alpha_F$ and $C_n - \alpha_F$ data is nearly linear as evident in Figure 6. This was expected based on the discussion in Section II and Equation (1) which shows a linear relationship between C_L and α_F. C_n and M_{FW} on a wind turbine are not influenced solely by the TEF but also by the vortices formed and shed at the trailing edge of the TEF-blade interface as explained by Miller and Quandt [18] and shown in Figure 2 from Section II. The newly formed vortices reduce the effective α on a small section of the blade thus reducing overall blade loading. This reduction could explain the smaller slope in the M_{FW} percent change data presented in Figure 6, particularly for $-\alpha_F$. This argument was also reported by Abdelrahman and Johnson [12].

To study turbine loading at a macro scale then it is sufficient to study M_{FW}. If there is a need to study the blade loading at a specific span-wise blade segment, then it is sufficient to study C_n. To study the turbine loading at a local scale, then it is important to study how the TEF changes surface pressure in the chordwise direction. To do so, a contour plot is used to present ΔC_p for $\alpha_F = -20°$ and 20° in Figure 7. As expected, ΔC_p is uniform versus azimuth (ψ) apart from a few variations due to flow non-uniformity. This non-uniformity and trend was also seen in the C_n plots in Figure 5c. Another interesting aspect of these plots is that the flap has more influence over ΔC_p close to the TE than the LE. This is aligned with the results and conclusions made from the 2D static results in Samara and Johnson [10]. All the isobars are shifted towards the TE as α_F decreases indicating that the flap does influence the aerodynamics along the entire chord length of the blade. In both contour plots, higher values of ΔC_p are concentrated at the leading edge indicating that the blade segment at *r/R*=0.82 is not stalled. In Figure 7.b, there exists a $+\Delta C_p$ region as indicated by the

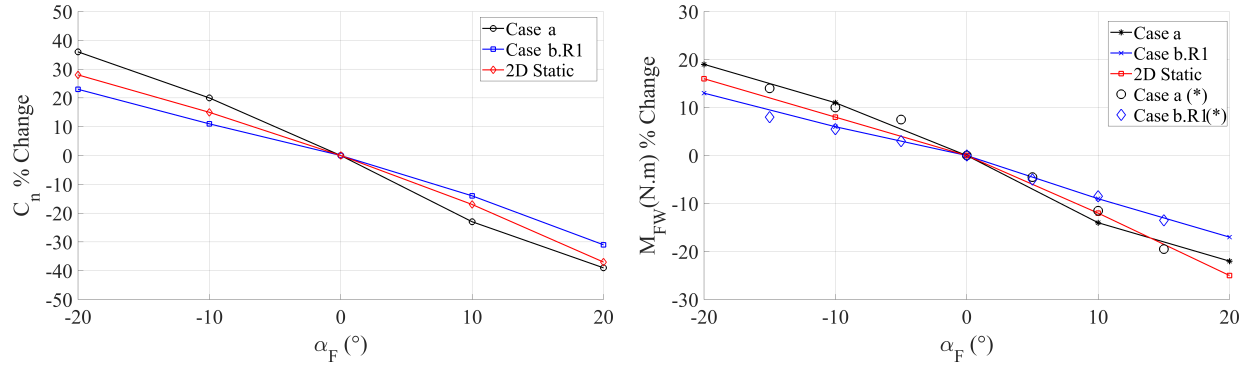

(a) % Change in C_n (b) % Change in Flapwise Moment (out of plane)

Fig. 6 Percentage change in a) C_n and b) M_{FW} relative to $\alpha_F = 0°$ for *Case a* and *b.R1* versus α_F where the flap is centered at *r/R*=0.82. (*) refers to experimental data points from Abdelrahman and Johnson [12].

isobar marked in white dashes at x/c=0.82. This occurs because as α_F is deflected to 20°, it creates a region around the flap hinge where the pressure is positive on the suction side of the airfoil. When $\alpha_F = -20°$ the mentioned region disappears so do the $+\Delta C_p$ values.

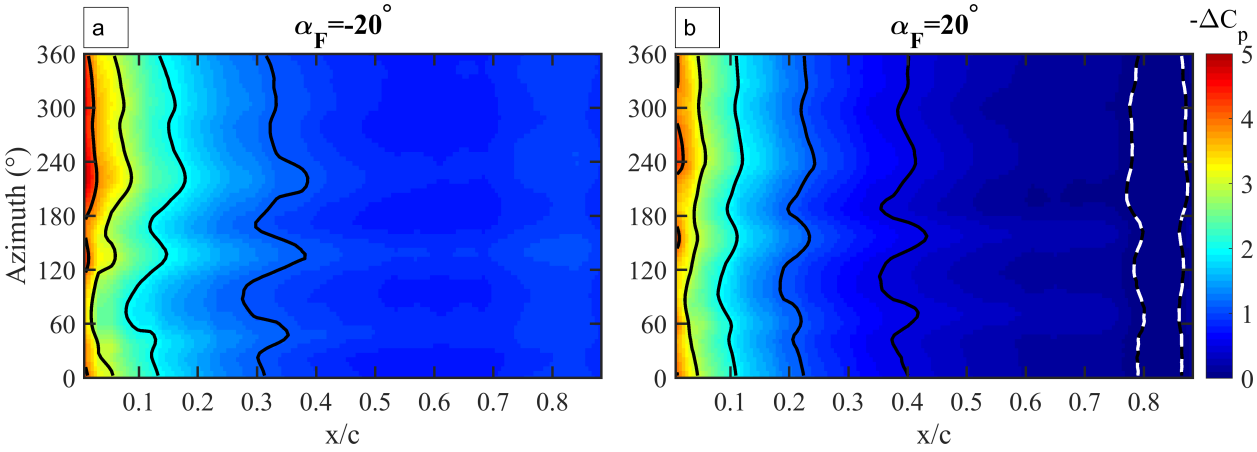

Fig. 7 Contours of $-\Delta C_p$ versus x/c versus ψ at *r/R*=0.82 for a) $\alpha_F = -20°$ and b) $\alpha_F = 20°$ for *Case b.R1* where λ = 3.5, $\gamma = 0°$, and $\beta = 3°$. The isobars on the plot represent constant $-\Delta C_p$ values=[0 0.5 1 2 3 4 5]. The isobar of $\Delta C_p = 0$ is marked in white dashes.

B. Yaw=0° Flap at *r/R*=0.66

In this section the flap location has been moved from *r/R*=0.82 to 0.66 to study how changing the flap location influences blade loading. From the previous section, it was concluded that the load variation with azimuth is negligible when $\gamma = 0°$. For this reason, the turbine performance parameters were averaged for the cycle and are plotted versus α_F and not versus azimuth. As a result of this plotting approach, different cases could be presented and compared in the same plot. The three performance parameters presented in Figure 8 are for four distinct cases identified in the plot legend where $\gamma = 0°$ and $\lambda = 3.5$. The red and black lines represent $\beta = 3°$ and 6° respectively, while the solid line

and the dotted line represent *r/R*=0.66 and 0.82, respectively. For all the cases presented, α_F ranged from -20° to 20° in steps of 10° but for *r/R*=0.66 and β = 3° (*Case b.R2*) additional α_F are presented for -80° to 80° in steps of 20°. Data for the extended α_F range was collected to investigate how extreme large α_F influences turbine loading. The two main discussion points are: how varying the TEF location changes its control capability; and how deflecting the flap to such high angles influences blade loading. First, ΔTorque is presented for the four cases in Figure 8a. Based on the α_F range of -20° to 20°, there is no clear trend or relationship between α_F and ΔTorque. The relationship is highly dependent on λ as seen in Figures 4 and 5 and is also dependent on β and *r/R* as seen in this figure. From the data discussed so far, it could be concluded that α_F influence over ΔTorque is not linear and the relationship is dependent on multiple external factors such as blade stall. A similar conclusion was also made by Samara and Johnson [11], which showed that the TEF was not capable of controlling rotor torque as effectively as blade pitch. Beyond $\alpha_F = \pm 20°$, ΔTorque diminishes for both extended α_F ranges because large values of α_F increase the drag coefficient at the blade section. Positive α_F produced the smallest ΔTorque values because the flow over the TEF blade section is severely stalled, significantly increasing the drag coefficient. Abbott and Von Doenhoff [29] in a 2D flow study clearly showed that $+\alpha_F$ does lead to higher drag coefficient when compared to $-\alpha_F$ and that in turn leads to lower ΔTorque values. When $\alpha_F = 80°$, ΔTorque is reduced by 31% and there should be an even greater reduction when the TEF *r/R* center increases to 0.82 because the moment arm and the velocity relative to the blade segment both increase making the drag force even larger and the lift force smaller. Johnson *et al.* [32] experimentally found that the highest power production area (area producing the most torque) is located at *r/R*=0.77 for the different cases they tested. This also indicates that the TEF centered at *r/R*=0.82 (flap located between *r/R*=0.73 and 0.91), is a better location to control ΔTorque than when the TEF is centered at *r/R*=0.66 (flap located between *r/R*=0.56 and 0.75). While not the focus of this study, the results presented here show that the TEF has the potential to assist the pitch control of utility-scale turbines. By doing so, the pitch control system will then be used less often thus increasing its lifespan and decreasing its maintenance and that could offset the cost of the TEF.

Second, M_{FW} is presented for the four cases in Figure 8b. Focusing on the operating range of $\alpha_F = \pm 20°$, the plot clearly shows that the relationship between α_F and M_{FW} is linear for all β angles, tip speed ratios and even when *r/R* is changed. When β decreased from 6° to 3°, the two M_{FW} data sets shifted upwards as expected but more importantly the slope of the data did not change. This is significant because it shows that the TEF control capability is the same when the turbine is operating under different conditions. Another important finding is that when *r/R*=0.82 the slope of the $M_{FW} - \alpha_F$ data for both β angles is steeper than *r/R*=0.66. The M_{FW}/α_F slope is equal to 3.6 Nm/10° when *r/R*=0.82 and is equal to 2.2 Nm/10° when *r/R*=0.66 and that is equivalent to a slope reduction of 40%. This clearly shows that when the TEF is centered at *r/R*=0.82, the control capability is significantly greater than when the TEF is centered at *r/R*=0.66. This was expected because Burton *et al.* [33] and Hau [34] both showed that the blade load per unit length in the flapwise direction increases steadily up to *r/R*≈0.92 where it is significantly reduced after that due to the tip loss

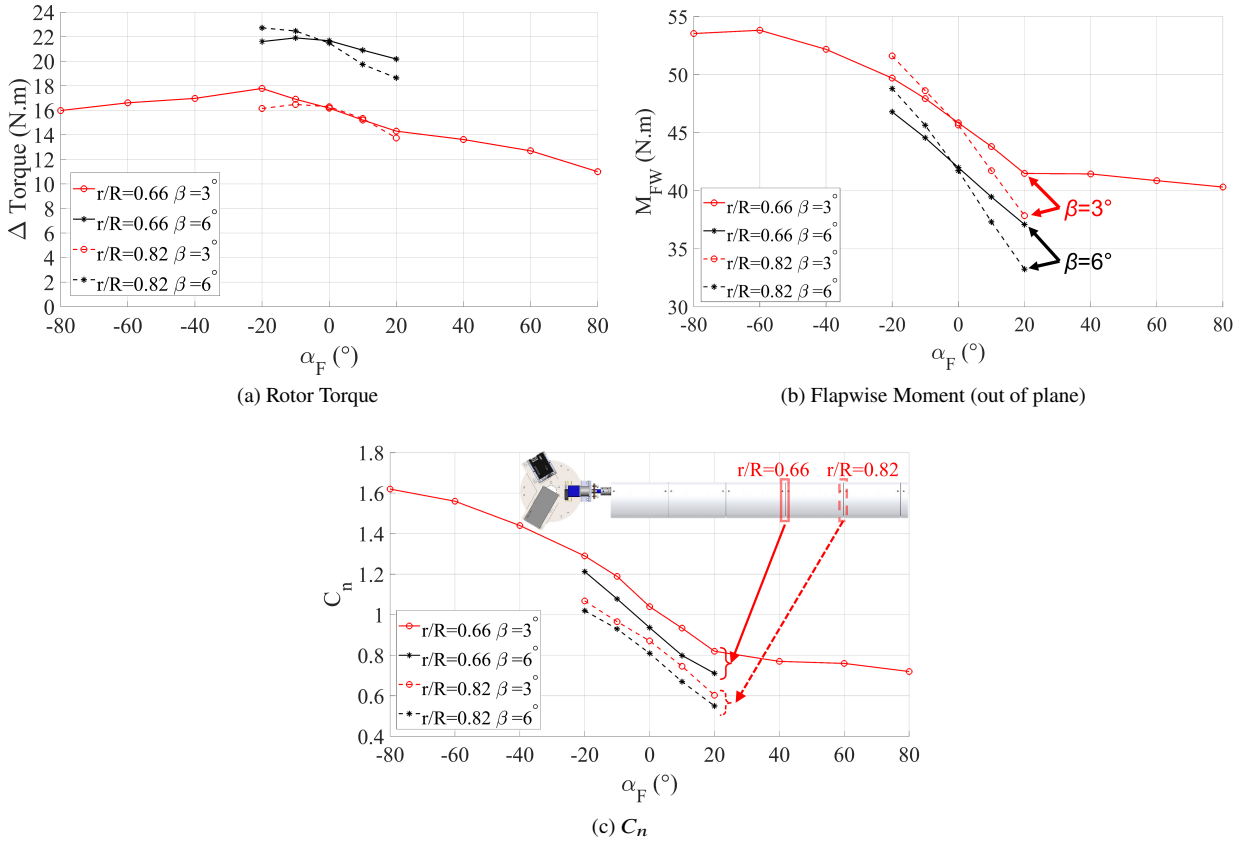

(a) Rotor Torque

(b) Flapwise Moment (out of plane)

(c) C_n

Fig. 8 Cycle-averaged turbine performance versus α_F for *Case b.R1* and *b.R2* where β = 3° and 6°, γ = 0°, λ=3.5 and the flap is centered at *r/R*=0.82 and 0.66.

effect. The M_{FW} magnitude is dependent on both the blade load and the moment arm. Since both of these variables keep increasing up to *r/R*≈0.92 then it makes most sense to place the TEF as close to this area as possible. When the TEF is centered at *r/R*=0.82 (flap located between *r/R*=0.73 and 0.91), it controls the loading on the blade segment that contributes most to M_{FW}. On the other hand, when the TEF is centered at *r/R*=0.66 (flap located between *r/R*=0.56 and 0.75), it controls the loading on the blade segment that contributes less to M_{FW}. Beyond α_F = ±20° range, the M_{FW} trend is no longer linear and it tapers off with no significant change in M_{FW}. This non-linearity exists because C_n is no longer linear outside the operating range and this is discussed in more detail after the C_n plots are discussed. Based on the evidence presented so far, the relationship between α_F and M_{FW} is linear as long as α_F = ±20°. This is in agreement with Berg *et al.* [17], Abdelrahman and Johnson [12], and Samara and Johnson [9].

Finally, the C_n data is presented for the four cases in Figure 8c. Focusing on the operating range of α_F = ±20°, the results are parallel to each other indicating a similar slope. This shows that the linearity between α_F and C_n is independent of *r/R* location, β angle, and tip speed ratio. This was also expected because from the static results published by Samara and Johnson [9], it was concluded that the influence of the TEF on C_n is linear for the entire range of α and

is not affected by the stall angle or other factors. Beyond $\alpha_F = \pm 20^\circ$ range, the trend is no longer linear as seen in Figure 8c. It is interesting to see that C_n keeps increasing as α_F decreases even at extremely large $-\alpha_F$ where it is expected that the blade section will be stalled. At large $+\alpha_F$, C_n does not continue to decrease as α_F increases. This trend in the data is explained better by looking at the ΔC_p contour plots presented next.

Similar to the ΔC_p contour plots presented in Figure 7 for *Case b.R1*, Figure 9 presents ΔC_p contour plots for α_F = [-80°, -20°, 0°, 20°, 80°] for *Case b.R2* where λ = 3.5, $\gamma = 0^\circ$, $\beta = 3^\circ$ and *r/R*=0.66. This provides a clear insight on how the pressure distribution changes with *r/R* location and for extreme α_F. When comparing Figures 9.b and d to Figure 7 where *r/R* decreased from 0.82 to 0.66, the $+\Delta C_p$ region present at $\alpha_F = 20^\circ$ is no longer present. This could be due to a change in Reynolds number and α increasing from 8° to 11° when *r/R* changed (α is obtained from Samara and Johnson [35]). For $\alpha_F > -20^\circ$, there is no indication from the contour plots, in Figure 9, that the blade segment is stalled since ΔC_p is concentrated at the LE. Differently, for $\alpha_F = -80^\circ$, ΔC_p is no longer concentrated at the leading edge and ΔC_p is significantly increased across the entire airfoil chord and this is indicative of stall. From the 2D static results in Samara and Johnson [9], it was found that even though the blade is stalled, C_L kept increasing similar to what is found here in the C_n data in Figure 8c. Another interesting case is $\alpha_F = 80^\circ$, where the flow is expected to separate but ΔC_p is still concentrated at the LE. For this reason, the trend in C_n tapered off in Figure 8c for large α_F. The measurements do not provide enough information to conclude with certainty whether the flow over the blade is stalled or not. What has been found is that 3D flow effects discussed in Samara and Johnson [35] have a significant impact on blade stall that typically leads to a less dramatic stall. More experiments and visualization are needed to study the dynamics of stall on a rotating blade.

C. Yaw=30° Flap at *r/R*=0.82

Similar to *Case b.R1* that was presented in Section IV.A, *Case c* is plotted in Figure 10 for the same condition but when the turbine is yawed. This way the influence of α_F on yawed turbine aerodynamics is studied and compared to the non-yawed cases. *Case c* also presents the opportunity to study how the TEF controls loads on a yawed turbine operating at the onset of stall where $\beta = 3^\circ$ and λ=3.5. The azimuth variation in all three variables with respect to α_F is very similar to what was found for the non-yawed turbine. This indicates that the TEF is capable of controlling turbine loading in yawed and non-yawed conditions in a similar fashion. This is important because utility-scale wind turbines spend the majority of their time in yawed conditions and it is essential for the TEF to attenuate cyclic loading in these different conditions [1]. The data presented so far shows that the TEF is capable of equally controlling the load on the turbine for different yaw angles, blade pitch angles, and wind speeds even when the turbine is operating at the onset of stall and the load fluctuations are high. Examining Figure 10 further, it could be seen that changing α_F keeps the load fluctuation magnitude and pattern about the same but the average load changes. It is concluded that changing α_F does not influence the possibility of stall contrary to what was found by Samara and Johnson [35] that a change in blade

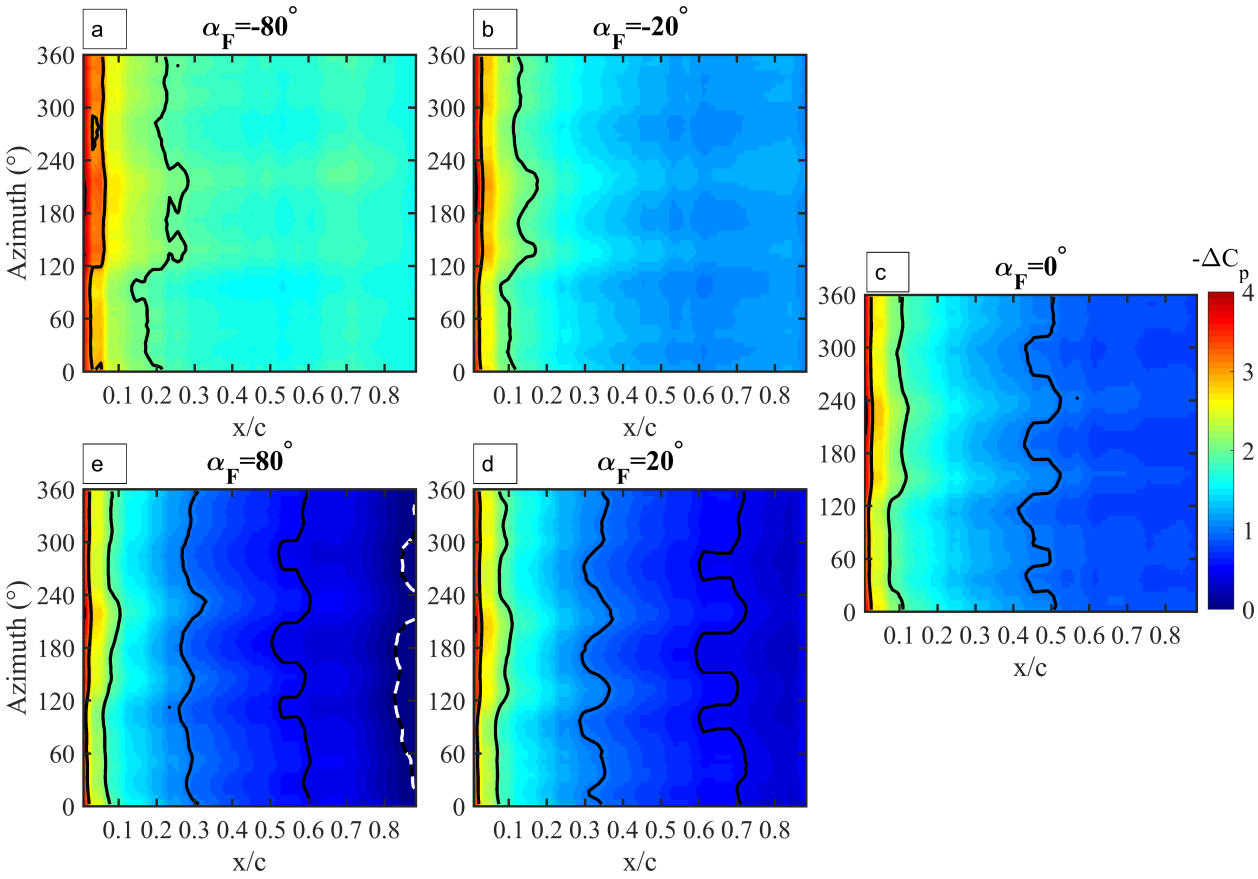

Fig. 9 Contours of $-\Delta C_p$ versus x/c versus ψ at *r/R*=0.66 for a) to e) α_F = [-80°, -20°, 0°, 20°, 80°] for *Case b.R2* where λ = 3.5, $\gamma = 0°$, and $\beta = 3°$. The isobars on the plot represent constant $-\Delta C_p$ values=[0 0.5 1 2 3 4]. The isobar of $\Delta C_p = 0$ is marked in white dashes.

pitch, β, significantly increases the possibility of blade stall. This suggests that it would be best to keep β constant and attenuate the loads using the TEF.

The contour plot in Figure 11 illustrates $-\Delta C_p$ versus x/c versus ψ for the minimum and maximum α_F when the turbine is yawed similar to the contour plots presented in Figure 7. When comparing Figure 11.a, $\alpha_F = -20°$, and 11.b, $\alpha_F = 20°$, there is an increase in ΔC_p across the entire chord of the airfoil, but the change in ΔC_p is more concentrated around the TE region. Similar to what was discussed in the non-yawed *Case b.R1*, there is a $+\Delta C_p$ region created around the flap hinge where the pressure is positive. This indicates that the flap is capable of significantly modifying the moment coefficient about the quarter chord.

The main aim of this article is quantifying the capability of the TEF in manipulating turbine loading. This is the first important step needed to determine how the TEF can alleviate cyclic loading on the turbine. Based on the results obtained from Sections IV.A and IV.B, the TEF is capable of manipulating M_{FW} by ±7.0 Nm and C_n by ±0.25 . From Section IV.C, when the turbine was yawed to an extreme angle of 30°, the cyclic loading in M_{FW} and C_n was found to be ±23 Nm and ±0.56, respectively. If the TEF motion was activated in such a way to reduce cyclic loading, then from

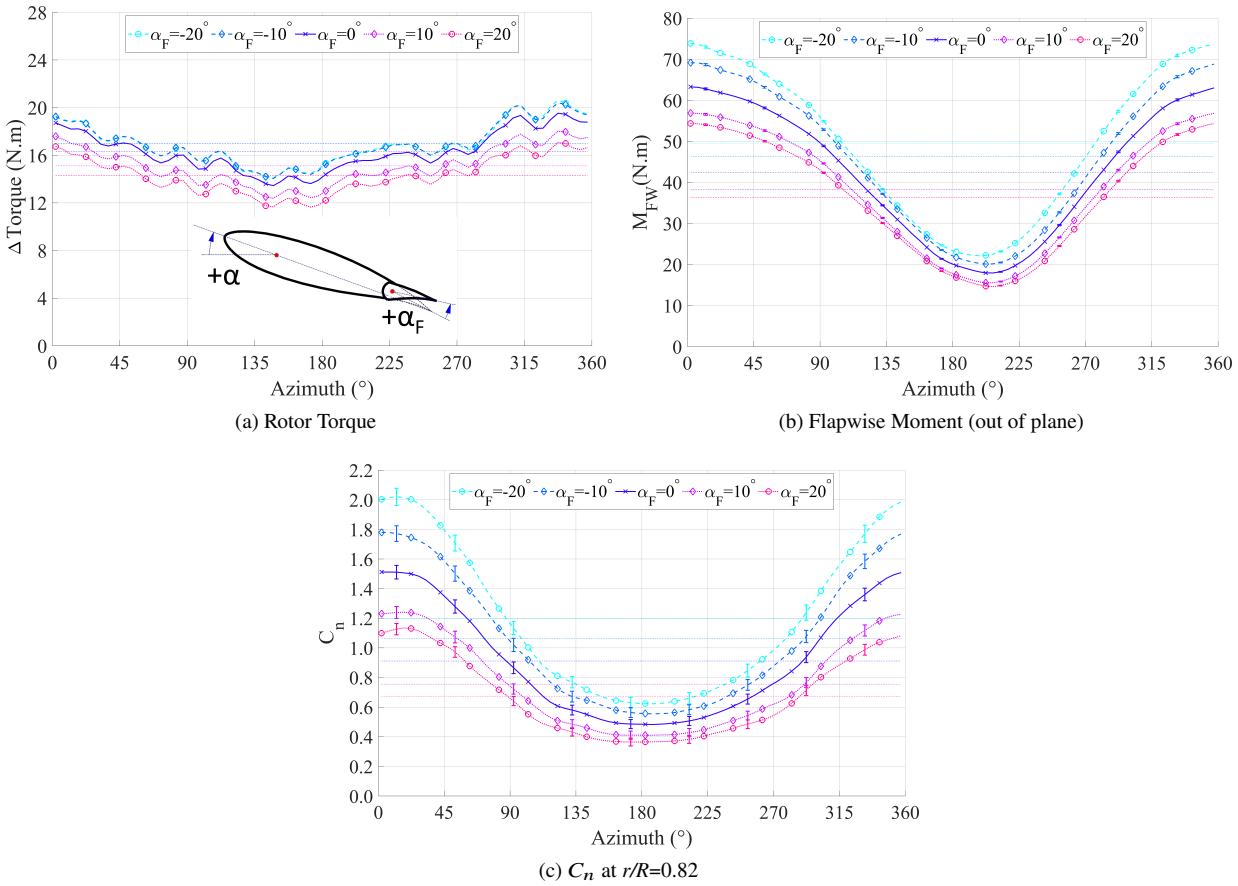

Fig. 10 Turbine performance for various α_F for *Case c* where $\beta = 3°$, $\gamma = 30°$, and λ=3.5. All data is plotted with only every 4th data point marked with a symbol for clarity.

the data just presented, it is expected for the cyclic loading in M_{FW} and C_n to be reduced by 30% and 47%, respectively. The mentioned cyclic loading reduction are estimates based on the data presented in this article. The current study proves that the TEF is fully capable of reducing cyclic loading on a wind turbine operating under yaw. To accurately measure the cyclic load reduction, then it is imperative to conduct experiments where the TEF is oscillating with the aim to attenuate cyclic loading. Subsequent studies by the same authors will aim to publish a study to address how an actively moving TEF can reduce cyclic loading based on the data presented here.

V. Conclusion

A unique set of data has been presented for different fixed trailing edge flap (TFE) angles (α_F) on an operating wind turbine in a large controlled wind facility. Measured parameters such as ΔTorque, flapwise bending moment (M_{FW}) and normal force coefficient (C_n) are plotted versus blade azimuth angle. The data is presented for a turbine operating under two different blade pitch angles (β), three different tip speed ratios (λ) and two yaw angles. The results showed that $-\alpha_F$ angles were capable of positively augmenting ΔTorque (turbine power output) in low wind speed conditions

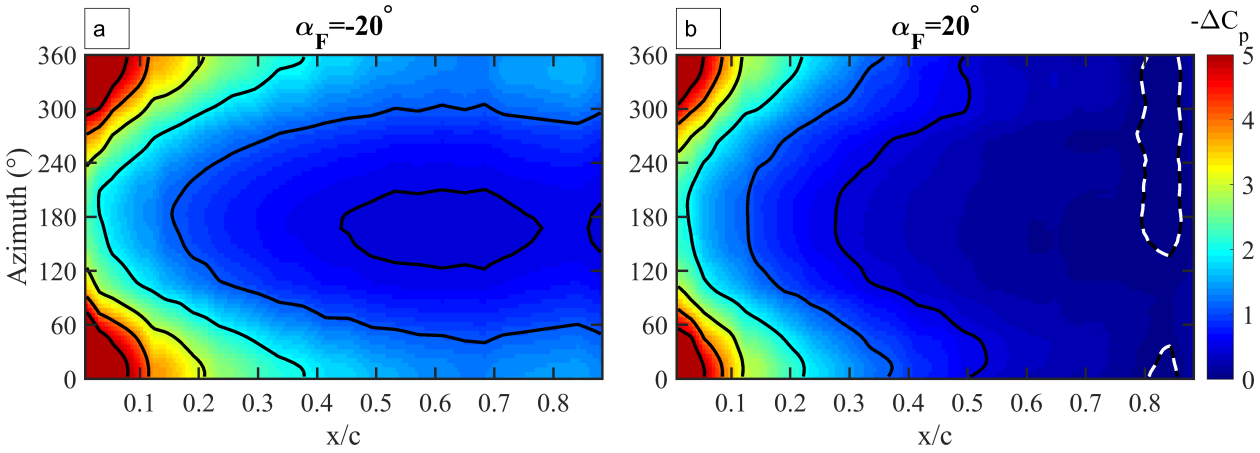

Fig. 11 Contours of $-\Delta C_p$ versus x/c versus ψ for a) $\alpha_F = -20°$ and b) $\alpha_F = 20°$ for *Case c* where λ = 3.5, $\gamma = 30°$, and $\beta = 3°$. The isobars on the plot represent constant $-\Delta C_p$ values=[0 0.5 1 2 3 4 5 6]. The isobar of $\Delta C_p = 0$ is marked in white dashes.

only and that is useful because the turbine power output is increased when it is typically producing less power. The measured wind turbine data showed that the control capability of $+\alpha_F$ is larger than the $-\alpha_F$ due to the maximum limit in C_n and the tendency of stall for high $-\alpha_F$. The data presented and analyzed here, from a scaled down wind turbine tested inside a wind tunnel, showed a very similar behavior to the data collected from a full scale wind turbine tested in the field. This would indicate that the physics obtained from a properly scaled-down wind turbine can indeed be used to obtain insight about full scale turbines as in this case.

After evaluating the TEF at two distinct *r/R* locations (0.66 and 0.82) and comparing the results under different wind turbine operating conditions, a few important conclusions could be made. It was found that the α_F influence over ΔTorque is not linear and the relationship is dependent on multiple external factors such as blade stall, λ, β and *r/R*. As for the relationship between α_F and M_{FW}, it is linear for all the cases presented whether the blade is operating under stall or not. The latter relationship also shows that when the TEF is centered at *r/R*=0.66 the control capability is reduced by 40% when compared to *r/R*=0.82. The linear relationship between α_F and C_n is constant and independent of *r/R* location, β angle, and tip speed ratio for the range studied. This is a crucial conclusion as it shows that the TEF is capable of controlling the load on the wind turbine for all operating conditions. For one of the cases presented, additional α_F were tested from -80° to 80° in steps of 20°. The data presented show that the TEF has the potential to assist the pitch control of utility-scale turbines by controlling the loading locally and at the root of the blade. For large α_F values, ΔTorque is reduced by 37% when α_F is deflected to -80° when the TEF is centered at *r/R*=0.66 and there should be an even greater reduction when the TEF *r/R* location increases to 0.82. Beyond the $\alpha_F = \pm 20°$ range, the relationship between $\alpha_F - C_n$ and $\alpha_F - M_{FW}$ is no longer linear because such high TEF angles causes the flow to separate over the blade. The TEF influence over turbine loading is no longer significant at extreme flap angles. This study indicates that the linear range of α_F for controlling turbine loading occurs when $\alpha_F = \pm 20°$ because in this range

the flow over the TEF is attached.

Turbine performance parameters were also studied for different α_F on a yawed turbine. It was found that the TEF is capable of equally controlling the load on the turbine for different yaw angles, blade pitch angles, and wind speeds even when the turbine blade is operating at the onset of stall and the load fluctuations are high. Based on the results presented, changing α_F keeps the load fluctuations about the same but the loads are increased or decreased contrary to changing β. This suggests that it would be best to keep β constant and attenuate the loads using the TEF.

From data presented, the TEF is estimated to reduce the cyclic loading in M_{FW} and C_n by 30% and 47%, respectively. This proves that if the TEF motion was activated, it can reduce cyclic loading and fatigue on multiple wind turbine components. With the help of active aerodynamic modification from the TEF, wind turbines can operate with a significant reduction in cyclic loading and therefore reduced fatigue levels. Future studies by the same authors will use the data presented here to develop a control strategy for the TEF to reduce cyclic loading while the turbine is yawed.

Funding Sources

The authors would like to gratefully acknowledge support from the Natural Sciences and Engineering Research Council of Canada (NSERC). Funding from the Ontario Graduate Scholarship to Farid Samara helped support this research.

Acknowledgments

The authors would like to thank Alison Zilstra for her help in running the experiments in the wind tunnel.

References

[1] Dykes, K., Veers, P., Lantz, E., and Al, E., "IEA Wind TCP: Results of IEA Wind TCP Workshop on a Grand Vision for Wind Energy Technology," Tech. Rep. IEA Wind TCP Task 11, National Renewable Energy Laboratory (NREL), 2019.

[2] Veers, P. S., Ashwill, T. D., Sutherland, H. J., Laird, D. L., Lobitz, D. W., Griffin, D. A., Mandell, J. F., Músial, W. D., Jackson, K., Zuteck, M., Miravete, A., Tsai, S. W., and Richmond, J. L., "Trends in the design, manufacture and evaluation of wind turbine blades," *Wind Energy*, Vol. 6, No. 3, 2003, pp. 245–259. https://doi.org/10.1002/we.90.

[3] Barlas, T. K., and van Kuik, G. A., "Review of state of the art in smart rotor control research for wind turbines," *Progress in Aerospace Sciences*, Vol. 46, No. 1, 2010, pp. 1–27. https://doi.org/10.1016/j.paerosci.2009.08.002.

[4] Shipley, D. E., Miller, M. S., and Robinson, M. C., "Dynamic stall occurrence on a horizontal axis wind turbine blade," *American Society of Mechanical Engineers, Solar Energy Division (Publication) SED*, Vol. 16, No. July, 1995, pp. 167–173. https://doi.org/10.2172/61151.

[5] Leishman, J. G., *Principles of Helicopter Aerodynamics*, 2nd ed., Cambridge University Press, 2006.

[6] Fleming, P. A., Ning, A., Gebraad, P. M., and Dykes, K., "Wind plant system engineering through optimization of layout and yaw control," *Wind Energy*, Vol. 19, No. 2, 2016, pp. 329–344. https://doi.org/10.1002/we.1836.

[7] Doekemeijer, B. M., Kern, S., Maturu, S., Kanev, S., Salbert, B., Schreiber, J., Campagnolo, F., Bottasso, C. L., Schuler, S., Wilts, F., Neumann, T., Potenza, G., Calabretta, F., Fioretti, F., and van Wingerden, J.-W., "Field experiment for open-loop yaw-based wake steering at a commercial onshore wind farm in Italy," *Wind Energy Science Discussions*, , No. June, 2020, pp. 1–22. https://doi.org/10.5194/wes-2020-80.

[8] Berg, D. E., Wilson, D. G., Barone, M. F., Resor, B. R., Berg, J. C., Paquette, J. A., Zayas, J. R., Kota, S., Ervin, G., and Maric, D., "The impact of active aerodynamic load control on fatigue and energy capture at low wind speed sites," *European Wind Energy Conference and Exhibition 2009, EWEC 2009*, Vol. 4, 2009, pp. 2670–2679.

[9] Samara, F., and Johnson, D. A., "Dynamic Stall on Pitching Cambered Airfoil with Phase Offset Trailing Edge Flap," *AIAA Journal*, 2020, pp. 1–13. https://doi.org/10.2514/1.j059115.

[10] Samara, F., and Johnson, D. A., "Deep dynamic stall and active aerodynamic modification on a S833 airfoil using pitching trailing edge flap," *Wind Engineering*, 2020. https://doi.org/10.1177/0309524X20938858.

[11] Samara, F., and Johnson, D. A., "In-Blade Measurements of Cyclic Loading on Yawed Turbines with Trailing Edge Flap," *Journal of Physics: Conference Series*, Vol. 1452, No. 1, 2020, p. 012061. https://doi.org/10.1088/1742-6596/1452/1/012061.

[12] Abdelrahman, A., and Johnson, D. A., "Development of a wind turbine test rig and rotor for trailing edge flap investigation: Static flap angles case," *Journal of Physics: Conference Series*, Vol. 524, No. 1, 2014, p. 012059. https://doi.org/10.1088/1742-6596/524/1/012059.

[13] Berg, D., Berg, J., White, J., Resor, B., and Rumsey, M., "Design, Fabrication, Assembly and Initial Testing of a SMART Rotor," *49th AIAA Aerospace Sciences Meeting*, Orlando, Florida, USA, 2011, pp. 4–7. https://doi.org/10.2514/6.2011-636.

[14] Berg, J., Berg, D., and White, J., "Fabrication, Integration and Initial Testing of a SMART Rotor," *50th AIAA Aerospace Sciences Meeting including the New Horizons Forum and Aerospace Exposition*, American Institute of Aeronautics and Astronautics, Reston, Virigina, 2012, pp. 1–9. https://doi.org/10.2514/6.2012-1291.

[15] Berg, J. C., Barone, M. F., and Resor, B. R., "Field test results from the Sandia SMART rotor," *51st AIAA Aerospace Sciences Meeting including the New Horizons Forum and Aerospace Exposition 2013*, 2013, pp. 1–10. https://doi.org/10.2514/6.2013-1060.

[16] Berg, J., Resor, B. R., Paquette, J., and White, J., "SMART Wind Turbine Rotor: Design and Field Test," *SAND2014-0681, Sandia National Laboratories*, , No. January, 2014. URL http://energy.gov/sites/prod/files/smart{_}wind{_}turbine{_}design.pdf.

[17] Berg, J. C., Barone, M. F., and Yoder, N., "SMART Wind Turbine Rotor: Data Analysis and Conclusions," *SAND2014-0712, Sandia National Laboratories*, , No. January, 2014. URL http://energy.sandia.gov/wp/wp-content/gallery/uploads/SAND2014-0712.pdf.

[18] Miller, L., Quandt, G. A., and Huang, S., "Atmospheric tests of trailing-edge aerodynamic devices," *National Renewable Energy Laboratory*, Vol. SR-500-223, 1998, pp. 1–45. https://doi.org/10.2172/565655.

[19] Andersen, P. B., Henriksen, L., Gaunaa, M., Bak, C., and Buhl, T., "Deformable trailing edge flaps for modern megawatt wind turbine controllers using strain gauge sensors," *Wind Energy*, Vol. 13, No. 2-3, 2010, pp. 193–206. https://doi.org/10.1002/we.371.

[20] Samara, F., "Active Aerodynamic Modification of Wind Turbine Blades to Reduce Load Fluctuation," Phd thesis, University of Waterloo, 2020. URL http://hdl.handle.net/10012/15760.

[21] Hand, M., Simms, D., and Fingersh, L., "Unsteady Aerodynamics Experiment Phase VI: Wind Tunnel Test Configurations and Available Data Campaigns," *National Renewable Energy Laboratory*, Vol. TP-500-259, No. 7, 2001, pp. 27–28. https://doi.org/10.1186/s12886-016-0364-4.

[22] Schepers, J. G., Boorsma, K., and Cho, T., "Final report of IEA Task 29, Mexnext (Phase 1): Analysis of Mexico wind tunnel measurements," *ECN Research*, Vol. Task 29, M, No. Phase 1, 2012, p. 312.

[23] Canet, H., Bortolotti, P., and Bottasso, C. L., "On the scaling of wind turbine rotors," *Wind Energy Science Discussions*, , No. March, 2020. https://doi.org/https://doi.org/10.5194/wes-2020-66.

[24] Bottasso, C. L., Campagnolo, F., and Petrović, V., "Wind tunnel testing of scaled wind turbine models: Beyond aerodynamics," *Journal of Wind Engineering and Industrial Aerodynamics*, Vol. 127, 2014, pp. 11–28. https://doi.org/10.1016/j.jweia.2014.01.009.

[25] Anderson, J. D., *Fundamentals of aerodynamics.*, 5th ed., McGraw-Hill Education, 1984. https://doi.org/10.2514/152157.

[26] Houghton, E. L., and Carruthers, N. B., *Aerodynamics for engineering students. Third edition.*, 5th ed., Butterworth Heinemann, 1982.

[27] Samara, F., and Johnson, D. A., "In-blade Load Sensing on 3D Printed Wind Turbine Blades Using Trailing Edge Flaps," *Journal of Physics: Conference Series*, Vol. 1037, No. 5, 2018, p. 052023. https://doi.org/10.1088/1742-6596/1037/5/052023.

[28] Gallant, T. E., and Johnson, D. A., "In-blade angle of attack measurement and comparison with models," *Journal of Physics: Conference Series*, Vol. 753, No. 7, 2016, p. 072007. https://doi.org/10.1088/1742-6596/753/7/072007.

[29] Abbott, I., and Von Doenhoff, A., *Theory Of Wing Sections*, Dover Publication Inc., 1959.

[30] Gallant, T., "Quantitative Measurement Techniques for Wind Turbine Blade Aerodynamic Performance," Master's thesis, University of Waterloo, 2017.

[31] Mckinnon, M., "Comparison of Experimental Methods in the Measurement of Wind Turbine Wakes," Masters thesis, University of Waterloo, 2018.

[32] Johnson, D., Abdelrahman, A., and Gertz, D., "Experimental indirect determination of wind turbine performance and blade element theory parameters in controlled conditions," *Wind Engineering*, Vol. 36, No. 6, 2012, pp. 717–738. https://doi.org/10.1260/0309-524X.36.6.717.

[33] Burton, T., Jenkins, N., Sharpe, D., and Bossanyi, E., *Wind Energy Handbook*, 2nd ed., Wiley, 2011. https://doi.org/10.1002/9781119992714.

[34] Hau, E., *Wind turbines: Fundamentals, technologies, application, economics*, 3rd ed., Springer, 2013. https://doi.org/10.1007/978-3-642-27151-9.

[35] Samara, F., and Johnson, D. A., "Experimental load measurement on a yawed wind turbine and comparison to FAST," *Journal of Physics: Conference Series*, Vol. 1618, 2020, p. 032031. https://doi.org/10.1088/1742-6596/1618/3/032031.